Theoretical Predictions of Temperature-Induced Gelation in Aqueous Dispersions Containing PEO-Grafted Particles

Xie, Fei; Woodward, Clifford E.; Forsman, Jan

Published in:
The Journal of Physical Chemistry Part B

DOI:
10.1021/acs.jpcb.6b01419

2016

Theoretical Predictions of Temperature-Induced Gelation in Aqueous Dispersions Containing PEO-Grafted Particles.

Fei Xie*, Clifford E. Woodward** and Jan Forsman* *

Theoretical Chemistry, P.O.Box 124, S-221 00 Lund, Sweden

***University College, University of New South Wales, ADFA Canberra ACT 2600, Australia*

E-mail: fei.xie@teokem.lu.se,phone:int+46462220381

Abstract

In this work we utilize classical polymer density functional theory (DFT) to study gelation in systems containing colloidal particles onto which polymers are grafted. The solution conditions are such that the corresponding bulk system displays a lower critical solution temperature (LCST). We specifically compare our predictions with experimental results by Shay *et al.*, who investigated temperature response in aqueous dispersions containing polystyrene particles (PS), with grafted 45-mer poly(ethylene oxide) (PEO) chains. Our DFT treatment is based on a model for aqueous PEO solutions that was originally developed by Karlström for bulk solutions. In this model, monomers are assumed to be in either of two classes of states, labelled A and B, where B is more solvophobic than A. On the other hand, the degeneracy of B exceeds that of A, causing the population of solvophobic monomers to increase with temperature. In agreement with experimental findings by Shay et al., we locate gelation at temperatures considerably below T_Θ, and far below the LCST for such chain lengths. This gelation occurs

*To whom correspondence should be addressed

also without any dispersion interactions between the PS particles. Interestingly, the polymer-induced interaction free energy displays a non-monotonic dependence on the grafting density. At high grafting densities, bridging attractions between grafted layers take place (considerably below T_Θ). At low grafting densities, on the other hand, the polymers are able to bridge across to the other particle surface. Shay et al. conducted their experiments at very low ionic strength, using de-ionized water as a solvent. We demonstrate that even minute amounts of adsorbed charge on the surface of the particles, can lead to dramatic changes of the gelation temperature, especially at high grafting densities. Another interesting prediction is the existence of elongated (chain-like) equilibrium structures, at low particle concentrations. We emphasize that our model does *not* rely upon any temperature-dependent interactions.

Introduction

A common way to prevent flocculation, or gelation, in particle dispersions, is to graft polymers onto the colloidal particles, i.e. through covalent attachment of end monomers to the particle surfaces. Under good solvent conditions, the repulsion between polymers will then tend to stabilize the dispersion.[1–5] However, solvent quality usually changes with temperature, so the stabilizing effects may be reduced or lost upon heating or cooling the system.[6–12] For instance, many polymer solutions display a lower critical solution temperature, LCST, and when such polymers are grafted onto particles, one may anticipate a decreased stabilization, as the temperature is increased.

Particles grafted with poly(N-isopropylacrylamide) have attracted a particular interest, since the LCST is close to human body temperature.[13–16] This makes such systems interesting candidates for drug delivery systems. Often, gelation is observed if the temperature is raised above the LCST.[13,15] Another important, and commonly used polymer, is poly (ethylene oxide), PEO, whose aqueous solutions also display an LCST.[17] In an interesting experimental study, Shay et al.[7] investigated stability and gelation of aqueous dispersions containing polystyrene (PS) particles, onto which they had grafted 45-mer PEO chains. In an aqueous bulk solution containing such short chains, there is a lower critical solution temperature of about 176 °C,[17] above which the solution

enters a demixing regime.

The theta temperature, T_Θ, which is the LCST for essentially infinite chain lengths, is roughly 90 °C for PEO in water.[17] Somewhat surprisingly, Shay et al. observed gelation well below the LCST. We can summarize their main experimental observations, as follows:

- Gelation (with 45-mers grafted on colloidal particles with a diameter of 250 - 300 nm) occurs at about 50 °C, i.e. far below the demixing regime for short chain PEG in water, and even well below T_Θ for that system (about 90 ° C).

- Reducing the grafting density promotes gelation, i.e. gelation then occurs at lower temperatures.

In this work, we will use a previously reported coarse-grained model for PEO[18,19] to generate a theoretical model for this system, which displays similar behaviours. A related model was used by Björling,[20] although he adopted the Scheutjens-Fleer theory,[21] and the study had a rather different focus to the present work. The parameters used in our model will not be specifically fitted to the experimental system. Instead, we aim to construct a generic model which is able to highlight the relevant underlying physics. Nevertheless, we have used the same particle size and polymer lengths as in the study by Shay *et al.* Furthermore, we borrow parameters from another work, where a coarse-grained model for PEO in water (at low temperatures) was developed.[22] Our work also includes some structural comparisons between DFT predictions and data from Monte Carlo simulations, for the coarse-grained model. It should be noted that our model does not contain any temperature-dependent interactions.

The model and the theoretical tools we will use, will be described in the next section. The following section gives a presentation of predictions and comparisons with experimental observations. The concluding section will provide a summary of our most important findings.

Model and theory

The PEO polymers will be modelled in a similar way to that described in earlier publications.[18,19] We assume that the monomers can be in either of two classes of states, labelled "A" and "B", with the former being solvophilic (having high polarity and/or hydrogen bonding ability), whereas the B monomers are solvophobic. The relative populations of the two classes of states are characterized by the ratio of the corresponding degeneracy factors, g_B/g_A. Quantum mechanical calculations[23] have estimated this ratio to be 11.5, and in our earlier work on this model, we set $g_B/g_A = 12$. We shall consider variations to that value in this work. This will be necessary, as the LCST vanishes for short enough chains, and with the model parameters that we have chosen, together with $g_B/g_A = 12$, the LCST disappears at a degree of polymerization, r, of about 80-90. Experimentally, the LCST persists down to about $r \approx 40-50$.[17] We obtain a better estimate for the behaviour of the LCST in our model, if we set $g_B/g_A = 13$. As Shay et al. grafted 45-mers onto their particles, and given that the LCST of the corresponding bulk polymer solution could be relevant, we have chosen to use $g_B/g_A = 13$ as the reference value for the population ratio. It should be noted that NMR studies of dimethoxyethane, dissolved in (highly polar) dimethylformamide[24] have demonstrated that the relative population of the more polar states decreases with increasing temperature. This lends some further support to our suggested parameters.

The polymer DFT we use has been described in earlier work,[18,19] but we provide a summary here, for completeness. We let $N(\mathbf{R})$ denote the density distribution of polymers with configuration $\mathbf{R} = \mathbf{r}_1, \mathbf{r}_2, ..., \mathbf{r}_r$, where $\mathbf{r}_i$ is the coordinate of monomer i. The monodisperse linear polymers contain r monomers, which are bonded together by an orientationally flexible bond potential V_b, chosen to ensure a constant bond length b. Hence, $e^{-\beta V_b(\mathbf{R})} \propto \prod \delta(|\mathbf{r}_{i+1} - \mathbf{r}_i| - b)$, where $\delta(x)$ is the Dirac delta function, and $\beta = 1/(kT)$ is the inverse thermal energy. Excluded volume effects are treated by imposing a local incompressibility constraint. Assuming a common monomer diameter σ, the sum of the density of monomers ($n_m(\mathbf{r})$), and implicit solvent particles ($n_s(\mathbf{r})$) is constrained to a fixed value. Hence, $n_t\sigma^3 = n_m(\mathbf{r})\sigma^3 + n_s(\mathbf{r})\sigma^3$, where we have set $n_t\sigma^3 = 1$. This model, which may be considered as a continuum space version of a lattice theory,[21] was introduced in an

earlier work.[25]

If we denote the probability distributions for monomers to be in class A or B states by $P_A(\mathbf{r})$ and $P_B(\mathbf{r})$, respectively, we can write the free energy functional, $\mathscr{F}$, as:

$$\begin{aligned}\beta\mathscr{F} &= \int N(\mathbf{R})\left(\ln[N(\mathbf{R})]-1\right)d\mathbf{R}+\beta\int N(\mathbf{R})V_b(\mathbf{R})d\mathbf{R}+\\ &\int(n_t-n_m(\mathbf{r}))\ln\left[n_t-n_m(\mathbf{r})\right]+n_m(\mathbf{r})d\mathbf{r}+\beta\mathscr{U}\left[n_m(\mathbf{r}),P_A(\mathbf{r})\right]+\\ &\int n_m(\mathbf{r})(1-P_A(\mathbf{r}))\ln\left[\frac{1-P_A(\mathbf{r})}{g_B}\right]d\mathbf{r}+\int n_m(\mathbf{r})P_A(\mathbf{r})\ln\left[\frac{P_A(\mathbf{r})}{g_A}\right]d\mathbf{r}+\\ &\beta\int(n_m(\mathbf{r})P_A(\mathbf{r})V_{ex}^{(A)}(\mathbf{r})+n_m(\mathbf{r})(1-P_A((\mathbf{r}))V_{ex}^{(B)}(\mathbf{r})+\\ &(n_t-n_m(\mathbf{r}))V_{ex}^{(s)}(\mathbf{r}))d\mathbf{r}+\int n_e(\mathbf{r})\Psi(\mathbf{r})d\mathbf{r}\end{aligned} \tag{1}$$

where we have included an external (surface) potential, $V_{ex}^{\alpha}(\mathbf{r})$, that acts on the α particles, with $\alpha = A$, B or s. The last term describes the grafting potential, $\Psi(\mathbf{r})$, which only acts on monomers $n_e(\mathbf{r})$, at one of the polymer ends. The functional $\mathscr{U}\left[n_m(\mathbf{r}),P_A(\mathbf{r})\right]$ describes attractive interparticle interactions:

$$\mathscr{U}\left[n_m(\mathbf{r}),P_A(\mathbf{r})\right]=\frac{1}{2}\sum_{\alpha,\beta}\int\int n_\alpha(\mathbf{r})n_\beta(\mathbf{r}')\phi_{\alpha\beta}^{(a)}(|\mathbf{r}-\mathbf{r}'|)d\mathbf{r}'d\mathbf{r} \tag{2}$$

with $n_A(\mathbf{r})\equiv n_m(\mathbf{r})P_A(\mathbf{r})$ and $n_B(\mathbf{r})\equiv n_m(\mathbf{r})(1-P_A(\mathbf{r}))$. The interparticle interactions $\phi_{\alpha\beta}^{(a)}(|\mathbf{r}-\mathbf{r}'|)$ are modelled by Lennard-Jones (L-J) potentials:

$$\phi_{\alpha\beta}^{(a)}(r)=4\varepsilon_{\alpha\beta}((\frac{\sigma}{r})^{12}-(\frac{\sigma}{r})^{6}),\qquad r>\sigma \tag{3}$$

Using ε_{AA} as a reference value, we define a reduced temperature $T^*=kT/\varepsilon_{AA}$, and reduced L-J parameters $\varepsilon_{\alpha\beta}^*\equiv\varepsilon_{\alpha\beta}/\varepsilon_{AA}$. We will use the same interaction parameters as in our earlier works on these systems:[18,19] $\varepsilon_{AA}^*=\varepsilon_{SS}^*=\varepsilon_{AS}^*=1$, $\varepsilon_{BB}^*=\varepsilon_{SB}^*=0.3$, and $\varepsilon_{AB}^*=\sqrt{0.3}\approx 0.55$. On a more technical note, all reduced energy levels were shifted one unit when performing calculations, since all *AA*, *AS* and *SS* interactions then vanish, thus reducing the computational cost. Such a global energy shift has no influence on the predictions, since all relative energy differences are maintained in the

incompressible model. Particle surfaces are simply modelled as planar, parallel walls, extending infinitely in the (x,y) directions, with the z axis defined as being normal to the surfaces. Imposing a mean-field assumption of uniform densities along the x,y directions, these dimensions are integrated out, leaving only z dependent quantities. The resulting interaction free energy per unit surface area (A), $g_s \equiv \int \mathscr{F} dxdy/A$, is then transformed into a corresponding interparticle potential of mean force between spheres, $W(D)$, using the Derjaguin Approximation:[26]

$$W(D) = -\pi R_s \int_D^\infty g_s(x)dx \tag{4}$$

where R_s is the colloidal particle radius, and D is the *surface separation* between the particles. As in earlier work, we tried to minimize the number of parameters by modelling the planar surfaces as hard, to solvent particles and monomers alike. Thus, $V_{ex}(z) = 0$, for $0 < z < h$, and infinite elsewhere. Finally, the grafting potential, $\Psi(z)$, which only acts on the monomer at the grafted (end) monomer of the polymers, is chosen in a similar manner, but in this case $\Psi(z) = \xi$ for $0 < z < \sigma$, and infinite elsewhere. The constant ξ acts as a Lagrange multiplier, and is adjusted to fulfill the external constraint imposed by the chosen grafting density, γ. We have simplified the system by minimizing the number of differently chosen parameters, many of which are set to be equal. In this manner we arrive at a relatively simple and generic model, which is physically reasonable. On the other hand, given that there is no "optimization" involved, we should not expect quantitative agreement with experiments.

Particles and grafting density

While our interaction parameters have not been fitted to the experimental results of Shay et al., we shall choose grafting densities and particle sizes which are consistent with their system. We set $\sigma = 3.1$ Å, so that σ^3 is equal to the volume per water molecule. The colloidal particles used in the system studied by Shay et al. had an estimated average radius of 140 nm, which is the value we use here. Furthermore, Shay et al. investigated systems with PEO to PS weight ratios

of 0.06 to 0.24 (denoted "L6" -> "L24" in their work). Assuming that *all* PEO chains during the synthesis ended up as grafted, suggests a reduced grating density, $\gamma^* \equiv \gamma\sigma^2$, in the range 0.008593 to 0.34372. These values were arrived at as follows. With a PS density of 1.05 g/cm^3, a colloidal particle has a mass of $[1.05*4*\pi*(140*10^{-7})^3/3]$ g. With a PEO monomer molecular weight of 44 g/mol, and a PEO to PS mass ratio of 0.06 (say), this suggests that (the maximum) number of grafted PEO chains on each particle is $N_{mon} = N_{Av}*0.06*1.05*4*\pi*(1.4*10^{-7})^3/(3*44)$, where N_{Av} is Avogadro's number. With 45 monomers per polymer this suggests that the polymer grafting density, γ, is $\gamma = N_{mon}/(45*4*\pi*1400^2)$ Å^{-2}, i.e. with $\sigma = 3.1$Å, $\gamma^* \approx 0.08593$. We stress that assuming that all available chains become grafted during the synthesis, could amount to a significant overestimation.

Structural comparisons with simulations

Before we make comparisons between theoretical predictions and experimental data, it is of interest to quantitatively evaluate our mean-field ansatz, and furthermore to adjust the bond length b, so as to generate a reasonable reference model for PEO in aqueous solutions at low temperatures, i.e in a good solvent. A simulation model has already been established, which reproduces experimental data for polymer radii of gyration and osmotic pressures, across many orders of magnitude.[22] This was achieved with a hard-sphere monomer model, in which the monomer diameter was set to 2.65 Å, with a bond length of 4 Å. In Figure 1, we compare results from simulations of grafted 45-mers, using these parameters, with DFT predictions, using the low temperature limit of our model (no L-J interactions), and a variable bond length. The simulated structures, which presumably provide a reasonable representation of grafted PEO in aqueous solution at low temperatures, are well captured by the DFT approach, across a wide range of grafting densities. Choosing $b = 1.75\sigma$ arguably leads to a slight overall improvement as compared with $b = 2\sigma$. Hence, we will use the former value in all DFT calculations reported below.

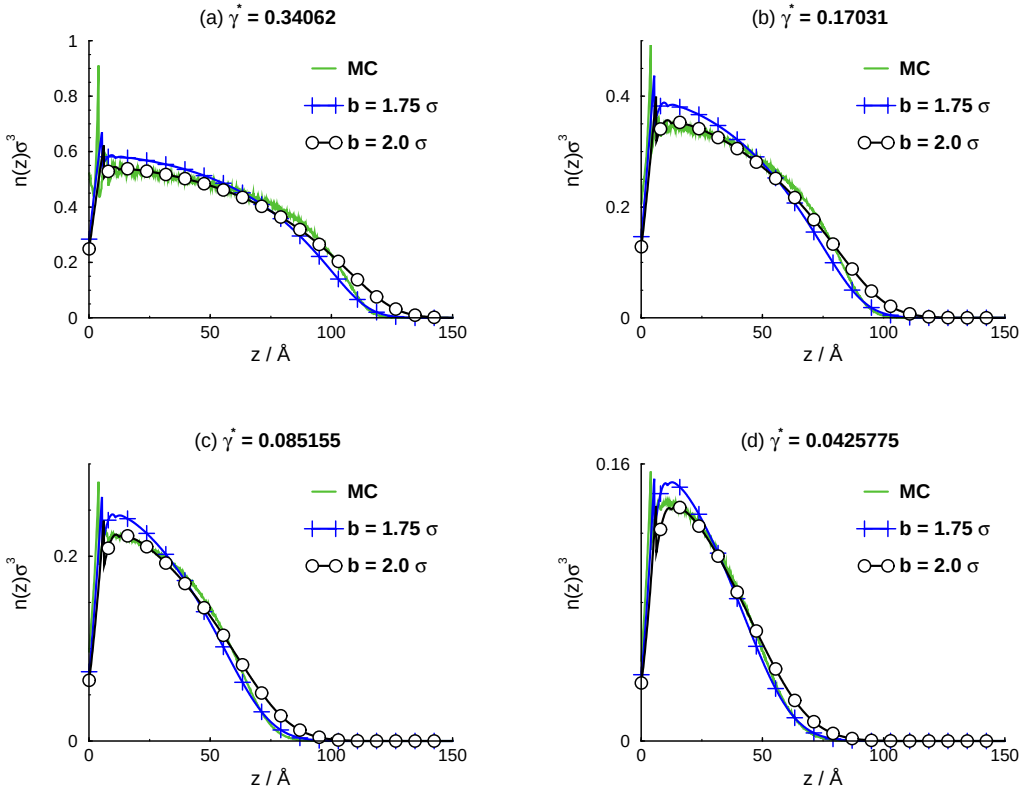

Figure 1: Structural comparisons between DFT predictions and simulations, under strictly good solvent conditions (no L-J interactions). The polymers are end-grafted to inert hard walls, at a reduced grafting density $\gamma^* \equiv \gamma\sigma^2$, with σ =3.1 Å. In the simulations, we have adopted parameters that have been shown to reproduce radii of gyrations and osmotic pressures across many orders of magnitude, in terms of polymer length and concentration, respectively.[22] Specifically, $b_{MC} = 4$ Å, and $\sigma_{MC} = 2.65$ Å. In the DFT calculations, we have set $\sigma = 3.1$ Å, since they are based on an implicit solvent approach (σ then represents a common effective diameter of solvent molecules and monomers). Two different choices for the reduced bond length, b, is tested.
(a) $\gamma^* = 0.34062$
(b) $\gamma^* = 0.17031$
(c) $\gamma^* = 0.085155$
(d) $\gamma^* = 0.0425775$

Bulk phase diagrams, and LCST

As mentioned earlier, we will consider two different choices of the degeneracy ratio, namely $g_B/g_A = 12$ and $g_B/g_A = 13$, with the latter being the prefered choice. The reason for this is that the experimental lower threshold molecular weight, for the existence of an LCST in aqueous solution, is close to 2000 g/mol, and with $g_B/g_A = 13$ we arrive at similar results. On the other hand, with $g_B/g_A = 12$, longer chains are needed to generate an LCST. In Figure 2, we show

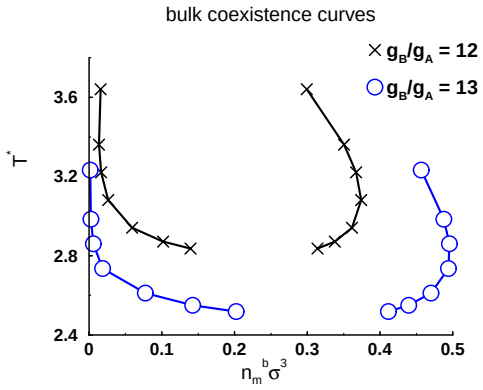

Figure 2: Predicted bulk phase diagrams, for 200-mers, with $g_B/g_A = 12$ and 13, respectively.

parts of the phase diagrams for 200-mers, with $g_B/g_A = 12$ and 13, respectively [1]. Here, we see how a larger degeneracy ratio clearly promotes phase separation. With $g_B/g_A = 12$, a degree of polymerization of about 80-90 is required to generate an LCST.

Results

As we evaluate the DFT predictions below, it is wise to keep in mind that the LCST for infinitely long polymers, which we denote as the Θ temperature, is about 2.44 when $g_B/g_A = 13$. For 45-mers (same length as the grafted chains), the LCST is $T^*_{LCST} = 2.837$. On the other hand, when $g_B/g_A = 12$, we arrive at $T^*_\Theta \approx 2.69$, whereas corresponding 45-mers do not generate any bulk phase separation.

Planar surfaces

Recall that the surfaces are inert and hard, with respect to all species (A, B, s). However, as we have illustrated in our earlier work, these solvophobic surfaces will effectively attract monomers, in particular those belonging to class B. The mechanism is analogous to the way in which hydrophobic

[1] Note that the phase diagram for the former system was also provided in Figure 2 of ref.,[18] but while the reduced temperature for the LCST, $T^*_{LCST} = 2.8007$ was correct, the rest of the phase diagram was not. Fortunately, this mistake, caused by a mixup of graphs, has no consequence for the conclusions drawn in ref.[18]

particles are "pushed" against hydrophobic surfaces in water. As we compare our predictions with experimental data, it is useful to introduce a "maximum" reduced grafting density, γ_r^*, which is the upper bound estimate of the most densely covered particles that was investigated by Shay et al. We shall use this value of $\gamma_r^* = 0.34372$ as our unit for grafting densities.

Interaction free energies: relation to grafting density and polymer length

In Figure 3, we display interaction free energies between planar surfaces, calculated for $g_B/g_A =$ 12 and 13, for a range of different grafting densities. The first thing to note is that, in agreement with the experimental observations of Shay et al., an attractive minimum exists for all grafting densities, even though the temperature in both cases is significantly lower than the theta temperature, and in the case of $g_B/g_A = 13$ *much* lower than the LCST for free 45-mers. We also observe

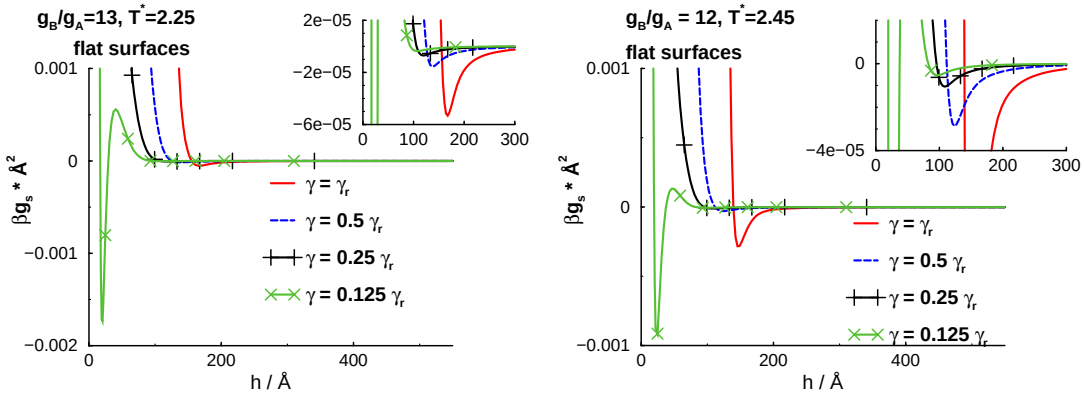

Figure 3: Predicted polymer induced interaction free energies per unit area (g_s), at various grafting densities, in a flat surface geometry.
(a) $g_B/g_A = 13$, $T^* = 2.25$ ($T_\Theta = 2.44$).
(b) $g_B/g_A = 12$, $T^* = 2.45$ ($T_\Theta = 2.69$).

interesting non-monotonic changes in the depth of this minimum, as the grafting density is varied. Specifically, at low grafting densities, we observe a strong, short-ranged attraction, while upon increasing γ, the attraction weakens, and is shifted to larger separations. However, an even greater increase of the grafting density generates a *stronger* minimum, located at even larger separations. This behaviour can be mechanistically rationalized as follows. At *low* grafting densities, there is enough space on opposing surfaces for polymers to bridge *across to the gap*. This bridging is

driven by solvophobic attraction, becoming more prevalent at high temperatures. This polymer-surface bridging attraction can be quite strong, but it is also short ranged, i.e., we anticipate significant bridging attraction at separations roughly corresponding to the thickness of one polymer layer. At *high* grafting densities, such bridging is prevented by steric hindrance from the opposing dense polymer layer. On the other hand, a similar bridging attraction can instead occur *between monomers that are bound to opposite surfaces*. Here we expect to see significant surface attractions at separations that roughly corresponds to two polymer layers. For our choice of interaction parameters, these bridges are typically weaker than those due to "surface bridging", at low grafting densities. Note that once the grafting density has become high enough to prevent bridging between surfaces, the attraction between polymer layers will become stronger as the grafting density increases, simply due to higher monomer concentrations of the opposing layers. This explains the initial decrease of the attractive minimum, as the grafting density is reduced from the "reference" value.

In addition to these considerations, we should also recognize that polymers are stretched in a dense layer, which also serves to increase the range of "interlayer bridging". This is highlighted in Figure 4, where we have plotted density distributions of free end monomers, at a moderately large

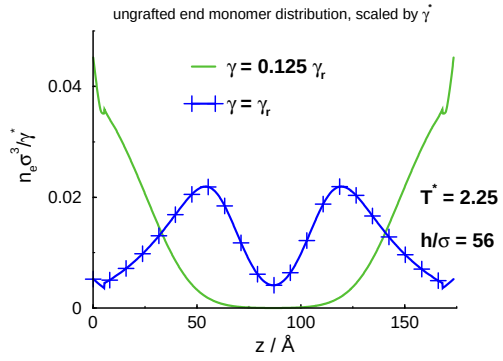

Figure 4: End monomomer density (n_e) distributions for high and low grafting densities, at T^* =2.25, and a flat surface separation of $h = 56\sigma$.

surface separation, and for low and high grafting densities. Notice that the two density distributions are *scaled* by the respective grafting density, i.e. their integral values are identical, allowing a

straightforward comparison. It is rather obvious that the polymers are considerably more stretched at the high grafting density, thus facilitating polymer mediated interactions at longer range.

Effects of curvature

Most of this work will be devoted to comparing DFT predictions with the experiments by Shay et al. In those experiments, large particles were used, so curvature effects were very small. It is nevertheless of interest to briefly demonstrate the DFT predictions of curvature effects, which will

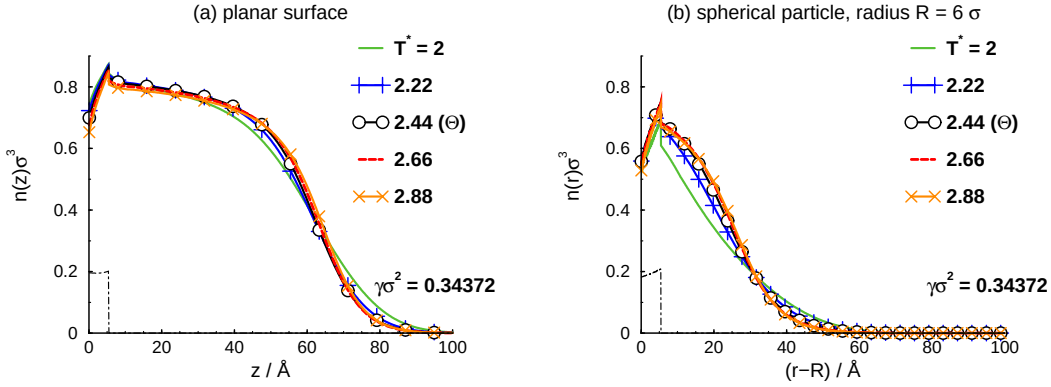

Figure 5: Comparing monomer density distributions at various temperatures, near a flat surface, and a spherical particle, respectively. The grafting density is high and identical, in both cases ($\gamma^* = 0.34372$). The distribution of the grafted end monomer (which is constrained to be within one σ from the surface, is also included, and indicated by a thin dashed black line
(a) Planar surface.
(b) Spherical particle, of radius $R = 6\sigma$.

be relevant to systems where the grafted particles are smaller. In Figure 5, we compare calculated density distributions at various temperatures, for polymers grafted to a flat surface and to a relatively small spherical particle. In the latter case, the DFT code was modified to account for the spherical symmetry. The grafting density is high, and the same for both cases. For these small particles (radius of 6 σ), curvature effects are quite pronounced. Since the available volume increases with distance for spherical particles, the density drops rapidly, and the effective polymer layer becomes considerably thinner, compared with the flat surface (or large spheres). We also note that most of the temperature response in the monomer density occurs substantially below the

theta temperature. Close to, and above, T_Θ, the structures are essentially temperature independent.

Dispersions containing spherical (0.28 μm) particles

Now we switch focus to interactions between spherical particles, of the same size as those investigated by Shay et al. We shall consider two different grafting densities, $\gamma = \gamma_r$, and $\gamma = 0.125\gamma_r$, which will simply be denoted as "high" and "low" grafting densities, respectively. These interactions are calculated using the Derjaguin Approximation.[26]

Neutral particles

In Figure 6, we show polymer-induced PMF:s between particles, at high and low grafting densities, and for a range of different temperatures. As we have already seen, the attraction, which is present

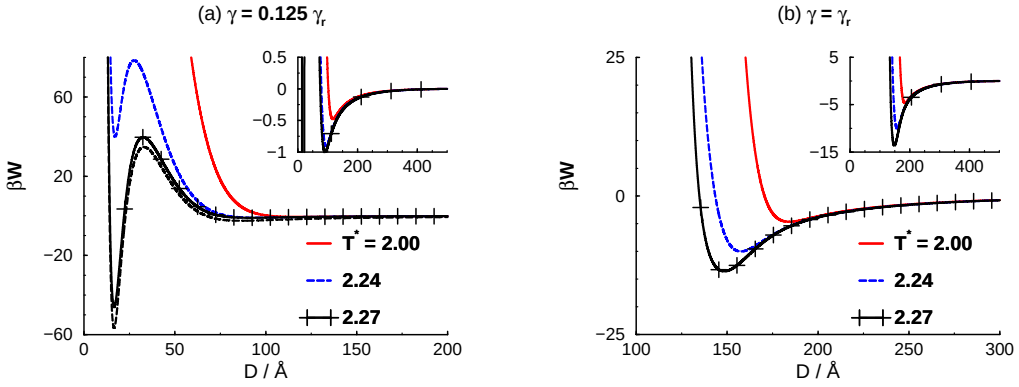

Figure 6: Potential of mean forces (W) between polymer-covered (grafted) particles, at various temperatures. The Derjaguin approximation has been utilized, and only polymer-induced interactions are accounted for.
(a) $\gamma = 0.125\gamma_r$
(b) $\gamma = \gamma_r$

far below the LCST for 45-mers (and below T_Θ), is considerably more long-ranged at high grafting densities. Shay et al. attributed the observed gelation to dispersion interactions, but our predictions suggest that these interactions only provide minor contributions, and are not required to explain the experimental results. An important observation is that while the surface to surface bridging, which dominates at low grafting densities, becomes very strong above some threshold (gelation)

temperature, this attraction vanishes much faster as the temperature drops, compared with the layer-layer bridging at high grafting densities. In other words, at low values of γ, the temperature dependence is quite strong.

In order to obtain gelation temperatures from our PMF predictions we have conducted canonical Metropolis Monte Carlo (MC) simulations on bulk solutions of hard particles, interacting with our calculated PMF:s. Specifically, we simulated 800 such particles, in a cubic simulation box of side length 45336 Å, applying periodic boundary conditions in all three dimensions. This gives a particle volume fraction of about 10 %, which is typical to the systems studied by Shay et al. A temperature increase from low values leads to more attractive PMF:s, as we have seen, and above a threshold temperature, clusters begin to form. This results in a connected (or partly connected) system, which we define as a gel. We evaluated the probability, $P_{part}(N_{cl})$, that a particle belongs to a cluster containing N_{cl} particles. A cluster is defined as a collection of particles, where each particle is within a distance R_c from at least one other particle in the collection. At high temperatures, the particle-particle radial distribution function displays a very strong nearest-neighbour peak, followed by an anti-correlated regime (where $g(r) < 1$). Typical rdf:s, slightly above and below the gelation temperatures, are shown in Figure 7. In both cases gelation occurs quite rapidly upon temperature increase, although more so at low grafting densities. In the experimental system, gelation was determined within an interval of 5 K, at low as well as at high grafting densities. This also indicated a rather strong temperature sensitivity, although further details are lacking, since Shay et al. did not report results with more narrow temperature increments. A choice for R_c is a value slightly beyond the nearest-neighbour peak, in the anti-correlated regime. While the choice of R_c is somewhat arbitary, this has little or no practical consequence, as any reasonable value leads to the same overall conclusions. We set $R_c = 3250$ Å, for high ($\gamma = \gamma_r$), and $R_c = 2850$ Å, for low ($\gamma = 0.125\gamma_r$) grafting densities. With these values for R_c, we stipulate that the system forms a gel if the maximum of $P_{part}(N_{cl})$ occurs for $N_{cl} \geq 4$. This is an arbitary definition, but gelation typically develops quite rapidly above some threshold temperature, T_g, so the precise definition of the transition point is unimportant. Typical behaviours of the probability distribution, $P_{part}(N_{cl})$,

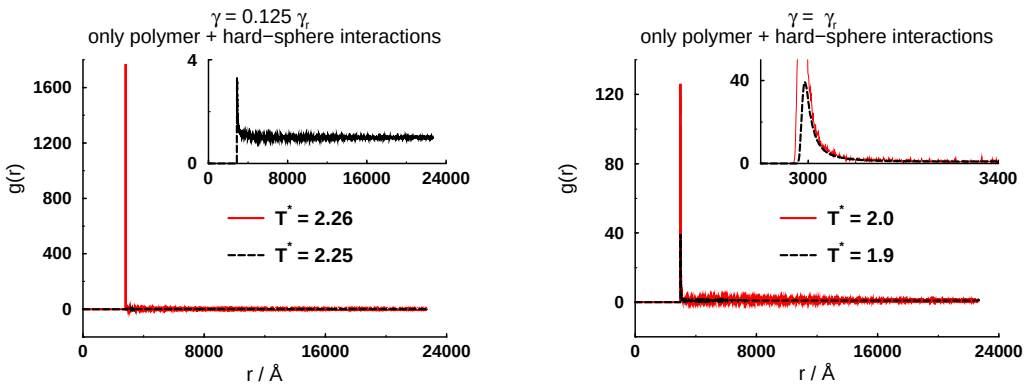

Figure 7: Radial distribution functions, $g(r)$, from simulations of particles interacting via polymer-induced PMF:s (as exemplified in Figure 6). Examples are given slightly above and below the gelation temperature.
(a) $\gamma = 0.125\gamma_r$
(b) $\gamma = \gamma_r$

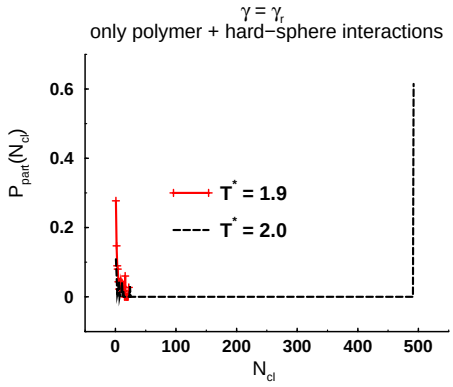

Figure 8: Probability distributions, $P_{part}(N_{cl})$, for a particle being a member of a cluster of size N_{cl}. The grafting density is high, $\gamma = \gamma_r$. Two cases are shown slightly below and above the gelation temperature. The interactions are purely polymer-induced (plus hard core), as illustrated in Figure 6).

in the vicinity of the gelation temperature T_g, are illustrated in Figure 8. Below T_g, at $T^* = 1.9$, the distributions display a maximum for monomers ($N_{cl} = 1$). However, a relatively small temperature increase, to $T^* = 2.0$, generates a dramatic response, with the maximum shifted to roughly $N_{cl} = 500$. This might actually be an underestimate, given that there is an upper system size limit of 800. Hence, we estimate that for this system, $1.9 < T_g^* < 2.0$.

Predictions of gelation temperatures, at low and high grafting density, respectively, are summa-

Table 1: Reduced gel temperatures, T_g^*, under various conditions. The particles always carry a hard core. In addition, they interact via grafter polymer mediated (pol.), with an optional addition of van der Waals (vdW) forces.

γ/γ_r	pol.	pol.+ vdW
1.0	$1.9 < T_g^* < 2.0$	$1.8 < T_g^* < 1.9$
0.125	$2.25 < T_g^* < 2.26$	$2.25 < T_g^* < 2.26$

rized in Table 1. In order to estimate the strength of dispersion (vdW) interactions, in units of kT, we have first of all assumed a Hamaker constant of $0.771 * 10^{-20}$ J, which is typical for PS-water-PS.[27] The transformation to thermal energy units is then facilitated by equating the theoretically predicted Θ temperature ($T_\Theta^* = 2.44$) to the experimentally observed one (about 363 K - see below), for aqueous PEO solutions. From Table 1, it is clear that vdW interactions only have a minor influence on these temperatures. There are at least two additional important observations to make. First, in accordance with the findings by Shay et al. gelation occurs substantially below the theta temperature. For PEO + water, the theta temperature is roughly 90 $^\circ$ C, i.e. 363 K - as estimated by a crude extrapolation of experimentally observed LCST:s to the case of "infinite" polymer length. Shay et al. found gelation at about 320-330 K, i.e. $T_g \approx 0.9 T_\Theta$. In our model system, the reduced T_Θ is 2.44, with a prediction of $T_g \approx 0.92 T_\Theta$ and $0.78 T_\Theta$ at low and high grafting densities, respectively. Overall, this is in reasonable agreement with experiments, especially considering that we use a rather coarse-grained generic model, with relatively few parameters. However, an important qualitative difference between our predictions and the experimental observations by Shay et al. is that they measured a gelation temperature which *increased* with grafting density, in the investigated interval, whereas we find the opposite trend, with our current model. One possible reason for this is that the PS particle surface attracts monomers more strongly than in our model, which can be modelled by introducing additional parameters. A decrease of the gelation temperature is expected with stronger monomer-surface interactions, particularly at low grafting densities, where surface to surface bridging dominates. While this is a rather straightforward explanation, there are other possible reasons for the discrepancy between our predictions and the findings by Shay et al. For example, the polymer grafting synthesis was followed thorough rinsing with de-ionized water, and subsequent experiments were also conducted in de-ionized water. A potential problem

with such an approach is that even minute amounts of adsorbed ions on the particles may generate significant interparticle interactions, due to the long range of electrostatic forces at such low ionic strengths. We shall therefore consider that possibility, and establish new predictions, under those conditions.

Weakly charged particles, low salt

Let us assume that there is a residual salt concentration of 0.01 mM (if the pH is higher than 9 or lower than 5, it is actually higher than that). Let us furthermore assume that the PS particles have some small extra affinity to (say) the anions, such that they effectively acquire a very weak surface charge density of $\sigma_s^{-1} = -200000$ Å$^2/e$. At a flat surface, this would imply an electrostatic intrinsic surface repulsion per adsorbed ion of $ł_B\pi \int_0^\infty \rho\sigma_s e^{-\kappa\rho}/\rho d\rho \approx 0.1$ i.e. 0.1 kT/charge (l_B is the Bjerrum length). Hence a rather small surface affinity would suffice. The presence of the weak surface charge means that an extra double layer force is added to the existing PMF interactions established above. These double layer interactions were solved using the non-linear Poisson-Boltzmann equation in our flat surface geometry[2]. These were then transformed to spherical particle interactions, using the Derjaguin Approximation. As we can see in Figure 9, the effects from such a seemingly minor ion-specific adsorption are quite dramatic (at low ionic strengths). At high grafting density, the temperature has to be increased quite considerably, in order for the polymer induced (layer-layer bridging) interactions to overcome the double-layer free energy barrier. The corresponding response is much weaker at low grafting densities, where we recall that the surface to surface bridging attraction grows quite rapidly with temperature. This means that a modest temperature increase will regenerate an attractive minimum at close range, even in the presence of long-ranged double-layer forces. However, this minimum will then be kinetically "protected" by a significant free energy barrier. Detailed studies of kinetic effects are outside the scope of this study, and by including random attempted displacements in the MC simulations, such free energy barriers can be efficiently crossed, allowing the system to reach equilibrium. Nevertheless, in an

[2] Although we prefer to formulate the problem using DFT, resulting in identical predictions.[28]

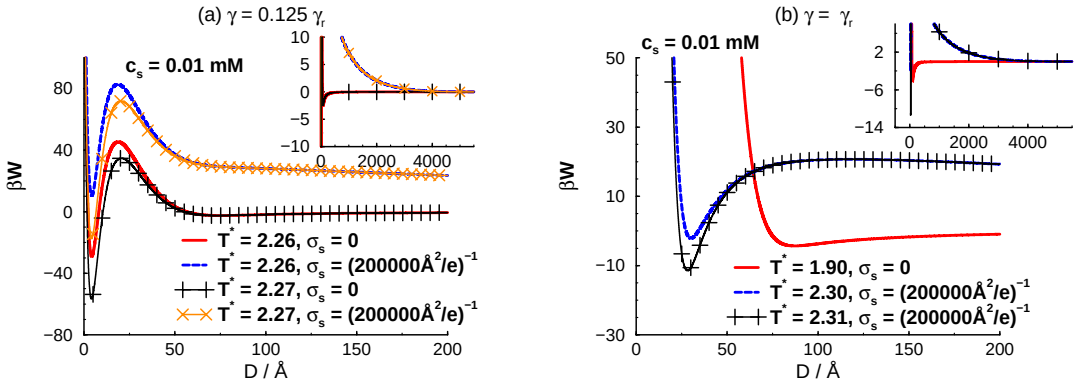

Figure 9: Potential of mean forces (W) between polymer-grafted particles, at various temperatures. The particles are also assumed to be very slightly charged, in a solution containing 0.01 mM simple monovalent salt. Typical vdW interactions have been added, assuming a Hamaker constant of $0.771 * 10^{-20}$ J. These have been transformed into kT units by equating the theoretical theta temperature, $T^*_\Theta = 2.44$ to the experimental value 363 K.
(a) $\gamma = 0.125\gamma_r$
(b) $\gamma = \gamma_r$

experiment, the barrier can have a significant effect on system dynamics.

In Table 2, we present a more complete table of gelation temperatures, now also including cases where double-layer interactions are added, as described above. The double-layer interactions have only a minor influence on T_g at low values of γ, but a major impact at high grafting densities. In the former case, the predicted T^*_g increases from the range 2.25-2.26 to 2.26-2.27 (including the vdW interactions), but at the high reference grafting density, the gelation range is shifted from 1.8-1.9 to 2.30-2.31. The presence of minute amounts of adsorbed net charge at low salt concentrations, qualitatively changes the dependence of the gelation temperature on the grafting density, causing it to follow the experimental trend.

Table 2: Reduced gel temperatures, T^*_g, under various conditions. The particles always carry a hard core. In addition, they interact via grafted polymer mediated (pol.), van der Waals (vdW) and electric Double Layer (DL) forces.

γ/γ_r	pol.	pol.+ vdW	pol. + vdW + DL
1.0	$1.9 < T^*_g < 2.0$	$1.8 < T^*_g < 1.9$	$2.30 < T^*_g < 2.31$
0.125	$2.25 < T^*_g < 2.26$	$2.25 < T^*_g < 2.26$	$2.26 < T^*_g < 2.27$

Equilibrium chains of weakly charged particles, at low ionic strengths

In the final part of this work, we make some structural predictions as yet not measured in experiments. The observed free energy barriers, brought about by a weak ion-specific adsorption and low ionic strengths, gives rise to the tantalizing possibility of creating polymer-like "equilibrium clusters", where the monomers are composed of PS particles. Such structures can form with the combination of a deep but short-ranged free energy minimum (at low grafting densities) and a long-ranged repulsion. These interactions tend to cause particles in a cluster to align themselves linearly, as this will reduce the overall repulsion, yet retain the attraction. We have investigated this system using MC simulations at a low particle volume fraction of $\phi_s = 1$ %. The temperature was chosen to be slightly above T_g, i.e. $T^* = 2.27$ and 2.31, at low ($\gamma = 0.125\gamma_r$) and high ($\gamma = \gamma_r$) grafting densities, respectively. In Figure 10, we present configurational snapshots from these simulations. We see that indeed, at low grafting densities, where the free energy minimum is deep but narrow, there is a clear tendency for the clusters to form chain-like structures. This tendency is, as expected, not present at high grafting densities. The formation of these "equilibrium polymers", would be interesting to test experimentally.

Summary and conclusions

In this article we have studied a model for PS particles with grafted PEO chains. The PEO monomers undergo configurational changes between solvophilic and solvophobic states, with the latter outnumbering the former. Hence in this model the PEO chains become less soluble at higher temperatures and bulk solutions display an LCST, which approaches the Θ temperature for very long polymers. When these polymers are grafted onto PS particles, there is evidence of bridging at temperatures well below the LCST for short polymers (45-mers). This bridging is caused by solvent expulsion, while the polymer fills the space between the particles. For low grafting density, the polymers attached to one particle are able to stretch to the surfaces of adjacent particles, leading to surface-surface bridging. At higher grafting density, polymers are unable to bridge across

Figure 10: Simulation snapshots of structures obtained at low volume fractions (1 %), in systems in which the grafted particles also carry a weak charge, in solutions containing 0.01 mM monovalent salt. Corresponding PMF:s are provided in Figure 9. The left graph shows a system with low grafting density, $\gamma = 0.125\gamma_r$, at $T^* = 2.27$. The right graph shows a system with high grafting density, $\gamma = \gamma_r$, at $T^* = 2.31$. In both cases, the temperature is slightly above the gelation temperature found at a particle volume fraction of 10 % (see Table 2).

the region between surfaces, due to steric hindrance, and instead there is an attractive bridging between the dense grafted layers. This attraction occurs at a larger separations than does surface-surface bridging. The occurrence of these attractive interactions are able to cause gelation of the PS particles at temperatures well below the LCST, for both sparsely and densely grafted particles. Experiments show that the gelation temperature is larger at higher grafting density, which is the opposite to what was found in our simple model. We have identified at least two ways by which the experimental results can be explained. Firstly, it is possible that an extra attraction exists between monomers and the PS surfaces, which increases the surface-surface bridging attraction at low surface coverage. Secondly, the PS particles may accumulate a small charge, which at the low electrolyte concentration conditions in the experiments, gives rise to a large double layer repulsion. This double layer repulsion has a stronger effect on the highly grafted system, which then raises its gelation temperature significantly. Finally, we note that it was not necessary to invoke temperature dependent interactions, or particle-particle dispersion forces to obtain a model that could explain experimental results.

Acknowledgement

J.F. acknowledges The Swedish Research Council for financial support.

References

1. Bridger, K.; Fairhurst, D.; Vincent, B. Nonaqueous silica dispersions stabilized by terminally-grafted polystyrene chains. *J. Coll. Int. Sci.* **1979**, *68*, 190 – 195.

2. Dunn, A. S. Polymeric stabilization of colloidal dispersions. By D. H. Napper, Academic Press, London, 1984 ISBN 0-12-513980-2. *British Polym. J.* **1986**, *18*, 278–278.

3. Zhulina, E. B.; Borisov, O. V.; Priamitsyn, V. A. Theory of steric stabilization of colloid dispersions by grafted polymers. *J. Coll. Int. Sci.* **1990**, *137*, 495 – 511.

4. Pincus, P. Colloid stabilization with grafted polyelectrolytes. *Macromol.* **1991**, *24*, 2912–2919.

5. Ueno, K.; Inaba, A.; Kondoh, M.; Watanabe, M. Colloidal Stability of Bare and Polymer-Grafted Silica Nanoparticles in Ionic Liquids. *Langmuir* **2008**, *24*, 5253–5259, PMID: 18426231.

6. Jansen, J.; de Kruif, C.; Vrij, A. Attractions in sterically stabilized silica dispersions: II. Experiments on phase separation induced by temperature variation. *J. Coll. Int. Sci.* **1986**, *114*, 481 – 491.

7. Shay, J. S.; Raghavan, S. R.; Khan, S. A. Thermoreversible gelation in aqueous dispersions of colloidal particles bearing grafted poly(ethylene oxide) chains. *J. Rheol.* **2001**, *45*, 913–927.

8. Zackrisson, M.; Stradner, A.; Schurtenberger, P.; Bergenholtz, J. Small Angle Neutron Scattering on a Core Shell Colloidal System: A Contrast-Variation Study. *Langmuir* **2005**, *21*, 10835–10845, PMID: 16262360.

9. Zackrisson, M.; Stradner, A.; Schurtenberger, P.; Bergenholtz, J. Structure, dynamics, and rheology of concentrated dispersions of poly(ethylene glycol)-grafted colloids. *Phys. Rev. E* **2006**, *73*, 011408.

10. Behrens, M. A.; Bergenholtz, J.; Pedersen, J. S. Temperature-Induced Attractive Interactions of PEO-Containing Block Copolymer Micelles. *Langmuir* **2014**, *30*, 6021–6029, PMID: 24850568.

11. Mao, H.; Pan, P.; Shan, G.; Bao, Y. In Situ Formation and Gelation Mechanism of Thermoresponsive Stereocomplexed Hydrogels upon Mixing Diblock and Triblock Poly(Lactic Acid)/Poly(Ethylene Glycol) Copolymers. *J. Phys. Chem. B* **2015**, *119*, 6471–6480, PMID: 25932653.

12. Li, M.; Pan, P.; Shan, G.; Bao, Y. Thermoresponsive poly(ε-caprolactone)-graft-poly(N-isopropylacrylamide) graft copolymers prepared by a combination of ring-opening polymerization and sequential azide - alkyne click chemistry. *Polym. Int.* **2015**, *64*, 389–396.

13. Barbier, V.; Herve, M.; Sudor, J.; Brulet, A.; Hourdet, D.; Viovy, J.-L. Thermally Induced Gelation of Poly(acrylamide) Grafted with Poly(N-isopropylacrylamide): A Small-Angle Neutron Scattering Study. *Macromol.* **2004**, *37*, 5682–5691.

14. Ohno, K.; Morinaga, T.; Takeno, S.; Tsujii, Y.; Fukuda, T. Suspensions of Silica Particles Grafted with Concentrated Polymer Brush:âĂL' A New Family of Colloidal Crystals. *Macromol.* **2006**, *39*, 1245–1249.

15. Zhang, Z.; Krishna, N.; Lettinga, M. P.; Vermant, J.; Grelet, E. Reversible Gelation of Rod-Like Viruses Grafted with Thermoresponsive Polymers. *Langmuir* **2009**, *25*, 2437–2442, PMID: 19166277.

16. Guo, X.; Du, Z.; Song, M.; Qiu, L.; Shen, Y.; Yang, Y.; Liu, X. Grafting thermosensitive PNIPAM onto the surface of carbon spheres. *Appl. Surf. Sci.* **2014**, *321*, 116 – 125.

17. Saeki, S.; Kuwahara, N.; Konno, S.; Kaneko', M. Upper and Lower Critical Solution Temperatures in Polystyrene Solutions. *Macromol.* **1973**, *6*, 246–250.

18. Xie, F.; Woodward, C. E.; Forsman, J. Fluid−Fluid Transitions at Bulk Supercritical Conditions. *Langmuir* **2013**, *29*, 2659–2666.

19. Xie, F.; Woodward, C. E.; Forsman, J. Non-monotonic temperature response of polymer mediated interactions. *Soft Matter* **2016**, *12*, 658–663.

20. Björling, M. Interaction between surfaces with attached poly(ethylene oxide) chains. *Macromol.* **1992**, *25*, 3956–3970.

21. Scheutjens, J. M. H. M.; Fleer, G. J. Statistical theory of the adsorption of interacting chain molecules. 1. Partition function, segment density distribution, and adsorption isotherms. *J. Phys. Chem.* **1979**, *83*, 1619–1635.

22. Xie, F.; Turesson, M.; Jansson, M.; Skepö, M.; Forsman, J. A simple and versatile implicit solvent model for Polyethylene Oxide in aqueous solution at room temperature. *Polymer* **2016**, *84*, 132–137.

23. Andersson, M.; Karlstrom, G. Conformational structure of 1,2-dimethoxyethane in water and other dipolar solvents, studied by quantum chemical, reaction field, and statistical mechanical techniques. *J. Phys. Chem.* **1985**, *89*, 4957–4962.

24. Viti, V.; Indovina, P. L.; Podo, F.; Radics, L.; Nemethy, G. Conformational studies of ethylene glycol and its two methyl ether derivatives. *Molec. Phys.* **1974**, *27*, 541–559.

25. Forsman, J.; Woodward, C. E. Surface forces in solutions containing rigid polymers: approaching the rod limit. *Macromol.* **2006**, *39*, 1269.

26. Derjaguin, B. V. Untersuchungen über die Reibung und Adhäsion, IV. *Kolloid Zeits.* **1934**, *69*, 155.

27. French, R. H.; Winey, K. I.; Yang, M. K.; Qiu, W. Optical Properties and van der WaalsLondon Dispersion Interactions of Polystyrene Determined by Vacuum Ultraviolet Spectroscopy and Spectroscopic Ellipsometry. *Aust. J. Chem.* **2007**, *60*, 251–263.

28. Forsman, J. A Simple Correlation-Corrected Poisson-Boltzmann Theory. *J. Phys. Chem. B* **2004**, *108*, 9236.